WDM laser transmitters for mobile free-space laser communications

Citation: Caplan, D. O., et al. "WDM Laser Transmitters for Mobile Free-Space Laser Communications." Proceedings Volume 9739, Free-Space Laser Communication and Atmospheric Propagation XXVIII, 13-18 February, 2016, San Francisco, California, edited by Hamid Hemmati and Don M. Boroson, SPIE, 2016, p. 97390W.

As Published: http://dx.doi.org/10.1117/12.2218297

Publisher: SPIE

Persistent URL: http://hdl.handle.net/1721.1/114865

Version: Final published version: final published article, as it appeared in a journal, conference proceedings, or other formally published context

WDM laser transmitters for mobile free-space laser communications

D. O. Caplan, R. T. Schulein, J. J. Carney, M. L. Stevens, S. J. Spector

D. O. Caplan, R. T. Schulein, J. J. Carney, M. L. Stevens, S. J. Spector, "WDM laser transmitters for mobile free-space laser communications," Proc. SPIE 9739, Free-Space Laser Communication and Atmospheric Propagation XXVIII, 97390W (22 April 2016); doi: 10.1117/12.2218297

SPIE.

Event: SPIE LASE, 2016, San Francisco, California, United States

WDM Laser Transmitters for Mobile Free-space Laser Communications[§]

D.O. Caplan[*a], R. T. Schulein[a], J.J Carney[a], M. L. Stevens[a], and S. J. Spector[b]

[a]MIT Lincoln Laboratory, 244 Wood Street, Lexington, MA 02420

[b]Draper Laboratory, 555 Technology Square, Cambridge, MA 02139

ABSTRACT

We describe the performance of versatile high-performance multi-rate wavelength division multiplexed (WDM) laser transmitters using next-generation compact high-extinction-ratio power-efficient (CHERPe) transmitter designs. These leverage periodic time-frequency windowing of directly modulated laser signals to efficiently generate nearly ideal WDM waveforms with only mW-class drive power, facilitating WDM-channelization and providing straightforward access to many THz of available optical spectrum with low-bandwidth electronics. Furthermore, this approach can support scalable multi-rate operation with good power- and photon-efficiency, which enables new architectural options. This approach is attractive for numerous applications and systems ranging from small airborne or CubeSAT-sized communication payloads to larger interplanetary lasercom platforms.

Keywords: free-space optical communications, optical transmitters, optical receivers, optical nonlinearities, integrated photonics

1. INTRODUCTION

Inadequate communication capacity increasingly limits deep-space exploration efforts and the utility of many airborne and satellite-based systems. Data rates of interest span more than 4-orders of magnitude, from the Mbit/s regime to 10 Gbit/s and beyond, and as rates get higher, conventional systems often become bandwidth constrained. Free-space laser communications is known to have great potential to overcome this bandwidth bottleneck[1-5].

Variable link losses, inherent to mobile free-space communication systems, are dependent on link distance, with diffraction-induced losses growing with the square of the link distance. For a given system, free-space diffraction losses can vary by some 10 to 15 orders of magnitude as link distances vary from 100s to 1000s of km (for aircraft and low Earth orbiting satellite constellations) to 100s of millions of km for interplanetary distances to Mars and beyond. Since achievable data rate is proportional to received power, communication systems often become power constrained as link-distance-induced losses grow.

Relative to state-of-the-art RF systems (e.g., the Mars Reconnaissance Orbiter[6-8]), proposed[9-11] and fielded[5, 12-14] lasercom demonstrations compare quite favorably – providing notably higher data rates with lower size, weight, and power (SWaP). These lasercom systems utilize a variety of designs, wavelengths, modulation formats, and transmitter (TX) technologies such as: 1.06μm master oscillator power amplifier (MOPA) TXs[15] using *M*-ary pulse-position modulation (*M*-PPM); 1.55μm MOPAs using *M*-PPM and differential phase shift keying (DPSK)[16-18]; narrow-linewidth 1.064μm designs using coherent phase shift keying (PSK)[13]; and 0.98μm/1.55μm directly modulated laser (DML) designs[14]. While the diversity of TX technologies highlights that many solutions are feasible, it also indicates the current lack of convergence or standardization, which could lead to compatibility issues and drive costs higher in the long run. Moreover, these successful lasercom demonstration systems were substantial, with mass > 30 kg and power > 100 W. These may not be easily reduced to the ultra-low-SWaP < 10 kg and 20 W payloads of interest for low-cost rapid-turn-around CubeSAT applications[19-21].

[§] This work is sponsored by the Assistant Secretary of Defense for Research & Engineering under Air Force Contract #FA8721-05-C-0002. Opinions, interpretations, conclusions and recommendations are those of the author and are not necessarily endorsed by the United States Government.

[*]doc@LL.MIT.EDU

Free-Space Laser Communication and Atmospheric Propagation XXVIII, edited by Hamid Hemmati, Don M. Boroson, Proc. of SPIE Vol. 9739, 97390W · © 2016 SPIE
CCC code: 0277-786X/16/$18 · doi: 10.1117/12.2218297

To address the bandwidth bottleneck limitations mentioned earlier, scalable wavelength division multiplexing (WDM) techniques can easily support higher data rates[22]. But, conventional multi-channel WDM TX implementations are often at odds with important design drivers for free-space optical (FSO) systems such as good receiver sensitivity, low SWaP, and reduced implementation complexity and cost. For example, in order to realize the benefits of using high-sensitivity M-ary orthogonal modulation formats such as *M*-PPM[23-30], high-fidelity TX waveforms with good modulation extinction ratio (ER) are required[27, 31-33]. DML TXs have the potential to be simple and SWaP-efficient, and can generate high ER > ~30 dB with reasonably low modulation drive power. However, this requires operating the laser below threshold, which limits modulation bandwidth to relatively low < ~100 Mbit/s-class rates. At higher ~Gbit/s-class rates, conventional methods for generating high-fidelity waveforms using external modulation can require several watts per channel[15, 16, 27, 33, 34], making it prohibitively expensive to scale to numerous WDM channels for SWaP-limited platforms.

In this paper, we describe implementation and performance considerations for a new class of low-SWaP WDM laser TXs using compact high-extinction-ratio power-efficient (CHERPe) TX designs[35-37]. These versatile high-performance TXs leverage periodic time-frequency windowing of directly modulated laser signals to efficiently generate nearly ideal high-ER WDM waveforms with only mW-class drive power per channel[35, 36]. This enables straightforward WDM-channelization and an efficient means of accessing many THz of available optical spectrum with low-bandwidth electronics. This improvement in scalability enables a single transceiver platform to support data rates from the Mbit/s regime to many tens of Gbit/s and beyond. Furthermore, compatibility with preamplified and photon-counting RXs, and high-speed operation over both free-space and fiber-optic channels could lead to broad applicability for these transceivers ranging from commercial telecom-type fiber systems to small airborne or CubeSAT-sized communication payloads to larger interplanetary lasercom platforms.

2. BACKGROUND

As shown in the theoretical capacity limits in Figure 1[26, 38, 39], improved sensitivity is possible with increased bandwidth expansion. Transceivers (TXs and RXs) that support high-sensitivity M-ary orthogonal formats such as *M*-PPM, frequency shift keying (M-FSK), and hybrid combinations can theoretically approach Shannon-limited sensitivities in the limit of large bandwidth expansion. Single photon-per-bit (PPB) class sensitivities can be achieved in theory over the additive white Gaussian noise (AWGN) channel[38] and fractions of a PPB over the Poisson-limited photon-counting channel[26, 39]. With efficient WDM access to many THz of optical spectrum, mobile FSO systems that can support both high data rates and high sensitivities can be envisioned.

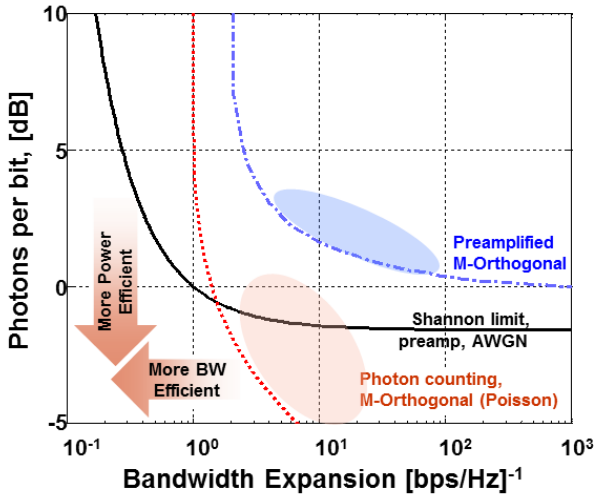

Figure 1. Theoretical trade between sensitivity (measured in photons/bit) and bandwidth expansion (measured in units of inverse spectral efficiency) for M-ary Orthogonal formats over the additive white Gassian noise (AWGN) and Poisson noise limited channels. Also shown is Shannon-limited capacity for the AWGN channel.

FSK is of particular interest relative to the more commonly used PPM because it has the same theoretical sensitivity advantage over binary formats but has *significantly lower peak power and electronic bandwidth requirements*. For both *M*-PPM and *M*-FSK, the sensitivity and the number of bits per symbol, $k = \log_2(M)$ grow with increasing *M* as does the spectral bandwidth, BW= $M/\log_2(M)$. *M*-PPM is relatively easy to implement at low data rates[27, 30, 38, 40], which helped motivate its selection as the modulation of choice for the Lunar Laser Communication Demonstration (LLCD) program[12]. However as seen in Figure 2a, for a constant data rate, the modulation rate for *M*-PPM, or corresponding electrical bandwidth, $BW_{M\text{-PPMelec}} = M/\log_2(M)$ grows with *M* as does the peak power. These were limiting design drivers for the LLCD uplink TXs[34, 41] and downlink RXs[42]. However, for *M*-FSK (shown in Figure 2b), the modulation rate (for a parallel WDM-based FSK transmitter) goes down as a function of *M*, with electrical bandwidth $BW_{M\text{-FSKelec}} = 1/\log_2(M)$. Moreover, the peak power is independent of *M* as can be seen in Figure 2b.

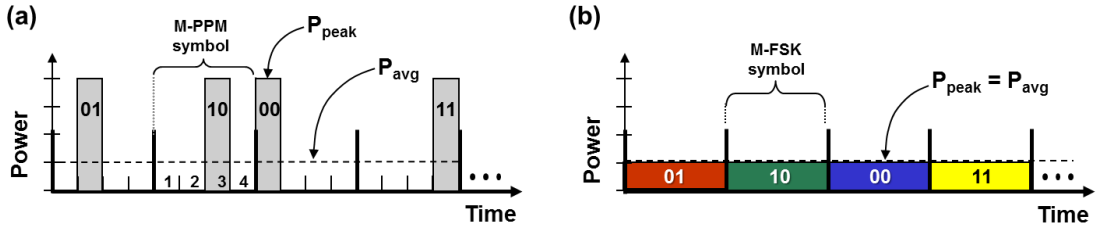

Figure 2. Two common orthogonal modulation formats: (a) M-ary pulse position modulation (*M*-PPM) and (b) frequency shift keying (*M*-FSK), shown for the case of *M*=4 and the number of bits per symbol k = 2.[33]

For hybrid formats with *f*-FSK frequency symbols and *p*-PPM positions, the effective number of bits per symbol,

$$k_{eff} = \log_2(p \cdot f) = \log_2(M_{eff}), \quad (1)$$

where M_{eff} is the effective cardinality of the hybrid 2-dimensional *p*-*f* symbol set[33]. In order to avoid power-robbing TX penalties, good modulation extinction ratio is needed with |ER| > M_{eff} + 15 dB required to keep power-robbing penalties below ~0.2 dB[33]. For example, with $p = 16$ and $f = 16$, k_{eff} = 8 bit/sym and M_{eff} = 256 (24 dB), so an ER > 39 dB is needed to avoid such TX penalties.

3. TRANSMITTER CONSIDERATIONS

The master oscillator power amplifier transmitter is the most commonly used design for high speed and high sensitivity applications. A conventional single-wavelength MOPA TX is shown in Figure 3 and includes a continuous-wave (CW) master oscillator laser, often implemented with a distributed feedback (DFB) laser; an external data modulator, which imparts the data onto the CW-optical carrier; a pulse-carving modulator, which cleans up the digitally modulated output, generating consistent high-quality pulsed waveforms; and the power optical amplifier, with output power sized to bridge the link of interest.

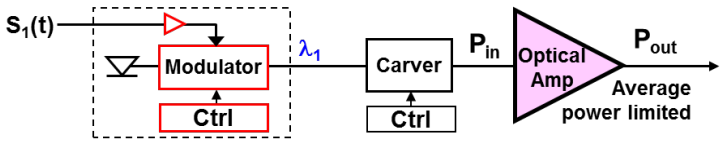

Figure 3. Single-channel master oscillator power amplifier (MOPA) transmitter, consisting of a CW source laser; external data modulator, driver, and stabilization control; narrow-band pulse carving modulator; and average-power-limited power amplifier.

The power amp often consumes a significant fraction of the overall transmitter power budget. At 1.55μm wavelengths, the MOPA power amplifier of choice is the erbium doped fiber amplifier (EDFA), which has wall plug power efficiency up to ~10% – 13%[43]. For example, an application requiring < 0.5 W TX power[11, 16-18, 44], might require ~5 W electrical power to run the EDFA. If the EDFA power dominates all other TX power requirements, then the net TX power efficiency converges to that of the power amp, which is the usually the best case for low-SWaP applications. However, while external modulators used in conventional systems can generate high-fidelity wide-band high-ER waveforms, the

accompanying external driver and bias control often require more than 4 W of electrical power, which is costly for low-SWaP systems that only need < ~0.5 W optical TX power. Furthermore, while extending this conventional approach to multiple WDM channels is straightforward, the 4 W cost for the external modulation of each channel would not be a scalable solution for SWaP-limited systems.

3.1 Directly Modulated Laser (DML) Transmitters

As noted earlier, DMLs have the potential for simple and efficient waveform generation, especially at low rates where the laser may be driven below threshold to achieve high ER. However, doing so generally leads to significantly chirped waveforms with highly broadened spectra that can be thousands of times larger than the transform-limited modulation. This, in turn, can lead to receiver limitations when operating in high background level environments. Furthermore, this approach does not scale well to higher modulation rates > 100 MHz. In the high-speed regime, DMLs are usually operated well above threshold. To improve modulation extinction ratio in this mode, larger modulation drive is used at the cost of higher-power Watt-class driver circuitry. This typically yields ER > ~10 dB, which is adequate telecom and datacom applications, but leads to substantial performance penalties that are prohibitive for many high-sensitivity applications that require ER > 30 dB[33, 45].

The use of optical filtering to improve DML ER has been previously investigated with a variety of filter-types including Fabry-Perot, fiber Bragg grating, and delay-line interferometer (DLI) filters, but only with ER < ~20 dB[46-49]. The ER-enhancement results from the fast adiabatic frequency-modulation (FM) or chirp induced by the direct laser modulation and subsequent AM/FM conversion performed by the optical filter[33, 46-49].

For a given FM-shift, narrow, higher-contrast filters provide better ER. Filter shape also plays an important role, with a broad passband and steep transition to a wide rejection band desired. For example, first-order DLI filters used by Vodhanel et al.[47], have a broad passband and a relatively steep transition, but they have a narrow stop band, which limits ER enhancement for wide-band modulation. However, by using a higher-order 2nd, 3rd, or 4th-order DLI, the 30 dB rejection bandwidth, (which is only ~3% of the free spectral range (FSR) for the 1st-order DLI), grows by a factor ~6, 10, and 15 times, respectively[50], dramatically improving the ER-enhancement. In another example, Fabry-Perot filters, and first-order micro-ring resonator (MRR) filters have a Lorentzian filter shape with a narrow pass band and gradual out-of-band roll off – with the 20 dB filter bandwidth being about 10 times the 3 dB full width half max (FWHM), making them poorly-suited for high-ER applications. But similar to the DLI example, using higher-order coupled MRR filters provides steeper roll-off and higher rejection relative to the FWHM as shown in the measured transmission spectra for 1st, 2nd , and 3rd-order MRRs in Figure 4a[50].

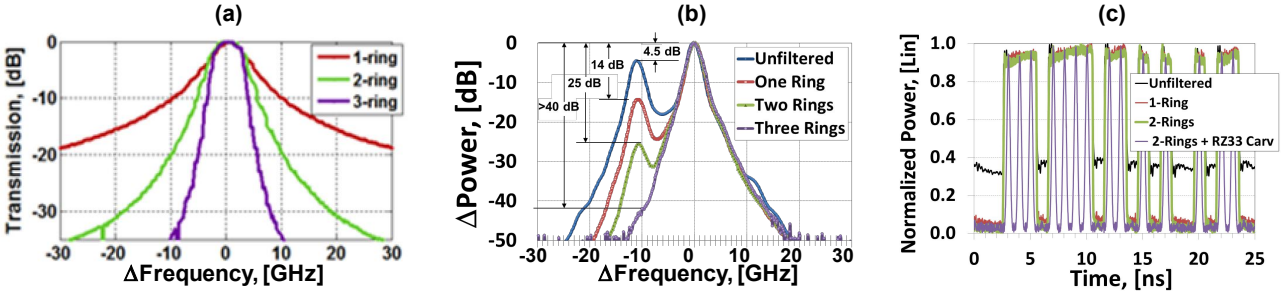

Figure 4. Measured microring resonator filter transmission spectra for 1, 2, and 3-ring filters. b) Measured DML spectra and ER with and without integrated MRR filtering. (c) Measured time-domain waveforms with and without MRR filtering, illustrating the ER improvement and undistorted 1-GHz PRBS output waveforms with filtering and pulse carving. Note that the time-domain measurements are limited by test-equipment noise, making it difficult to distinguish between the high-ER 1-ring and 2-ring filtered waveforms that are more easily distinguished in the filtered spectra measurements which have a higher dynamic range.

Such MRR filters can be fabricated in silicon with sub-100μm-class feature sizes and ~6 GHz FWHM passbands. Relative to the 1-ring MRR, the 2-ring and 3-ring filters provide about 10 dB and 25 dB more rejection, respectively at 10 GHz from the pass-band center[50]. As shown in the optical spectrum analyzer (OSA) measurements of DML transmission spectra in Figure 4b[50], the steeper rejection of the higher-order filters results in significant ER improvement. The average ER of the modulated signal is only 4.5dB without filtering; and increases to ~14 dB, 25 dB,

and 40 dB with increasing filter-order. Time domain measurements in Figure 4c, show ER improvement without any noticeable distortion of the 1 GHz pseudo random bit sequence (PRBS) modulated waveforms. Pulse carving further improves waveform uniformity and generates return-to-zero (RZ) waveforms that facilitate matched filtering in the RX[33]. Note that test equipment noise-limitations prevent direct time-domain observation of ER > ~13 dB[50].

The FSR of high contrast filters like these can be made so that a single passive optical filter may be used to process multiple WDM TX signals simultaneously. When combined with a periodic pulse carver as shown in Figure 5a, a two dimensional time-frequency window is formed (Figure 5b), which can further improve ER and generate nearly-ideal transform-limited output waveforms. Moreover, proper selection of the periodic filter-carver transfer function can minimize the impact of noise on the modulation signal, improving output waveform fidelity in the presence of noisy input drive waveforms[35-37]. Representative 2-ring MRR filtered and 33% RZ pulse-carved waveforms are shown in Figure 4c. The result of this is the ability to generate high-fidelity high-ER WDM waveforms at GHz-class modulation rates with modulation power < ~20 mW/channel[35, 36]. This enables a variety of scalable low-SWaP modulation options such as WDM-OOK, WDM-M-PPM, M-FSK, and M-orthogonal PPM/FSK hybrids. The hybrid options are attractive for many reasons. For instance, the number of orthogonal positions (*p*) and frequencies (*f*) and independent WDM wavelengths (*w*) can be adjusted to provide the best high-sensitivity option for the data rate and link of interest, providing an additional lever to accommodate for modulation bandwidth and peak power limitations[33].

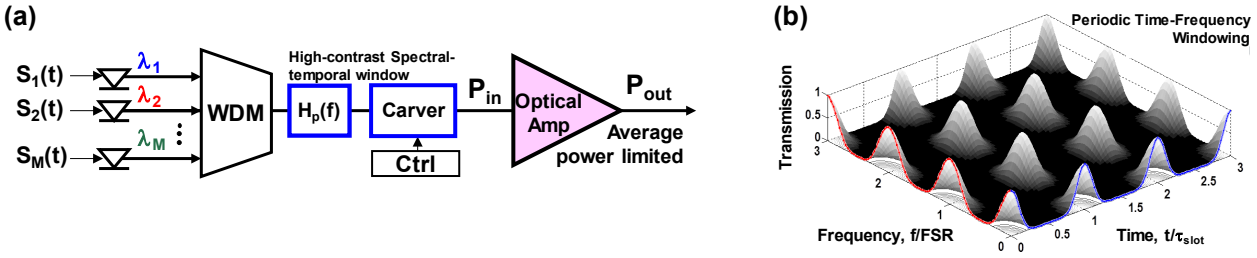

Figure 5. (a) WDM master oscillator power amplifier (MOPA) transmitter leveraging the compact high extinction ratio power efficient (CHERPe) modulation approach. $H_p(f)$ is a passive periodic optical filter that works in concert with the periodic pulse-carver to generate a high-contrast spectral-temporal window. (b) Representative time-frequency windowing function performed by the periodic filter-carver pair.

3.2 WDM Transmitter and Filter Integration

Notable improvements in SWaP may be obtained through transmitter integration. For example, by incorporating *N* lasers into a single transmitter optical assembly (TOSA), there is potential for an *N*-fold reduction in the number of power-hungry elements such as thermo-electric coolers (TECs), that can draw 1-W class power to stabilize the temperature and wavelength of the master laser. With modulation drive power significantly reduced, the master-laser TEC power can be a substantial amount of the remaining TX power budget. Reducing this by a factor of *N* would facilitate scalability considerably. Figure 6a shows an example 8-channel WDM TX prototype, with single TEC, single mode fiber output, and CHERPe DML bandwidth > 1.25 GHz with < ~20 mW drive power per channel. With these characteristics, a pair of these 8-channel devices could, for example, support high-sensitivity 16-FSK at rates up to 5 Gbit/s and high-rate WDM-OOK up to 20 Gbit/s. The proposed 16-channel TX would require less than 0.5 W of modulation power, and have drive levels low-enough to be driven directly from the high-speed FPGA outputs[36].

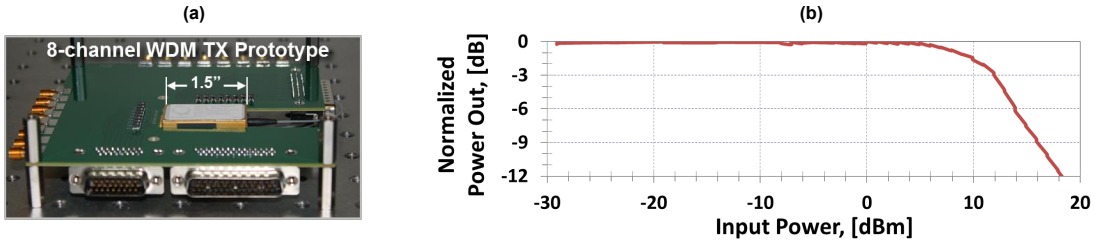

Figure 6. (a) 8-channel WDM TX prototype. (b) Measured power handling for a 3-ring integrated silicon microring resonator filter, with a nonlinear cutoff power > 1 mW average[50].

Leveraging photonic integration is another potential area for SWaP and cost reduction, by decreasing size while increasing versatility and functionality. When considering resonant silicon-based devices such as the MRRs mentioned above, it's important to consider the power handling capabilities. Figure 6b shows measured power handling characteristics for the 6 GHz 3-ring integrated MRR fabricated in silicon. The normalized output power is unchanged through ~0 dBm input power. At higher power, the transmission begins to decrease due to thermal shifting of the resonant frequency of the filter[50]. The output power level needs to be sufficient to drive a subsequent high-gain TX power amplifier, which can be designed to operate efficiently with -10 dBm input power[17]. Extending this to M-FSK waveforms, where one channel is always 'on', would have little impact on these nonlinear limitations. However the use of low-duty-cycle waveforms such as *M*-PPM could result in different nonlinear limitations that could impact both average and peak-power-limited transmission characteristics due to effects such as two-photon absorption, and free-carrier absorption and refraction effects that are still under investigation.

4. RECEIVER CONSIDERATIONS

The good waveform fidelity and high extinction ratio waveforms from the WDM CHERPe TXs enable many high-sensitivity receiver options including both photon counting and optically preamplified RXs. Here, we focus on preamplified RXs that are compatible with both space-based and terrestrial operation, and highlight some example RX configurations that enable the straightforward demodulation of *M*-FSK optical waveforms. Figure 7 shows a representative transceiver, with a CHERPe-based WDM TX on the left and preamplified RX on the right. Key RX elements include a low-noise EDFA preamplifier, periodic optical filter, polarizer, WDM filter, an *M*-FSK demod section followed by the decoder – decision circuitry. The low-noise preamplifier typically has > ~40 dB gain to provide enough optical signal to overwhelm subsequent thermal noise in the detection process. To remove out-of-band amplified spontaneous emission (ASE) and background noise, a narrow-band periodic filter with bandwidth matched to the incoming signal waveform is used to filter all the WDM input channels. The polarization beam splitter can be used to separate polarization division multiplexed signals and remove orthogonally polarized ASE from the single-pol signal. Next, the WDM coarse filters, separates, and passes the amplified narrow-band-filtered signals to the *M*-FSK Demod section.

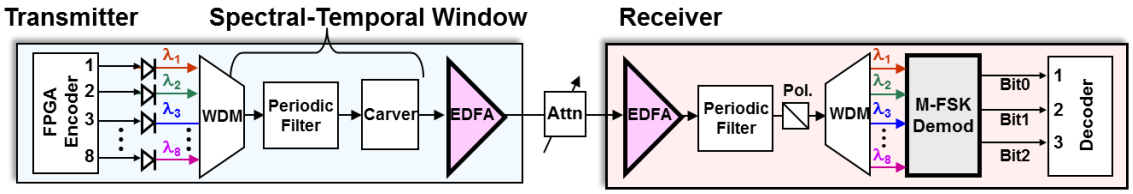

Figure 7. CHERPe-based WDM-MOPA transmitter (left) and preamplified WDM receiver (right). The M-FSK demod section can be configured to demodulate the incoming M-ary FSK signals prior to the k-bit decoder.

Optimal demodulation of *M*-FSK requires determining which of the *M* incoming waveforms is largest. For the binary case of 2-FSK, this can be achieved with a demod section that simply directs the two WDM-separated optical signals to a pair of detectors and performs a binary comparison as shown in Figure 8a. For $M > 2$, optimal demodulation can be implemented with *M* analog-to-digital converters (ADCs) to quantify each of the *M*-WDM separated signals so that comparison can be performed digitally. However, since ADCs are more complex, require more power, and have lower bandwidth than simple binary comparators – it is attractive to consider more scalable binary-comparison-based approaches for SWaP-efficient RXs. Figure 8b and Figure 8c show example demod sections that perform the demodulation function for 4-FSK and 8-FSK, respectively[35, 36, 51]. For the 4-ary case, the demod section takes in the 4 WDM input to a 'quad' 4x4 input/output block that distributes and combines them incoherently using 50/50 splitters such that two binary comparisons can be used to determine the 2-bits of logical output data per symbol. For the 8-ary case, the demod section is more complex – containing 2-quads and a third combination stage – but performs a similar distribution and combination function such that 3 binary comparisons can be used to determine the 3-bits of logical output data per symbol. This approach scales to 16-FSK and beyond, with $\log_2(M)$ binary comparisons needed to determine the *k* bits of logical data per symbol. As seen in Figure 8a-c, the demod section gets progressively more complex as *M* grows. But, while the complexity is fairly onerous when implemented with discrete components, it is well suited for integrated photonic solutions currently under development.

Independent of *M,* the demod section performs a distribution function that can be implemented with elements that are passive, low-power, and wide band. In fact, the entire receiver chain can be implemented entirely with elements that are readily available with bandwidths > 40 GHz. For 16-FSK with 4-bits/per symbol, this corresponds to data rates up to 160 Gbit/s, showing that these RX technologies have the potential for both sensitive and wide-band operation.

Note that while this binary demodulation approach avoids the use of *M*-ADCs, it is suboptimal for $M > 2$. However, the additional penalty is relatively small for $M \leq 16$, both in theory and practice when implemented with nearly matched optical filtering.[35, 36] With the addition of a single high-speed ADC that samples the optical power prior to the WDM, time-dependent signal-amplitude information is obtained that can be used to demodulate waveforms such as *M*-PPM and hybrid *p*-PPM/*f*-FSK modulated waveforms discussed in Section 3. The ADC sample information may also be used to improve performance by providing input to a soft-decision forward-error-correction (FEC) decoder.

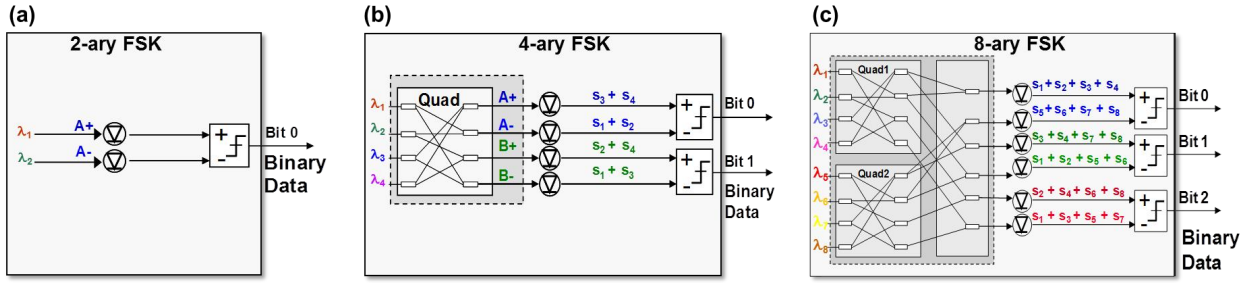

Figure 8. Example demod sections that perform the demodulation function for (a) 2-FSK, (b) 4-FSK, and (c) 8-FSK optical waveforms with an approach that can extend to 16-FSK and beyond[35, 36].

5. PERFORMANCE

The bit-error rate (BER) for ideal preamplified *M*-ary orthogonal modulation is shown in Figure 9 as a function of received power in dB photons/bit, for *M* between 2 and 256. Consistent with the theoretical capacity curves in Figure 1, sensitivity continues to improve with *M*, but with diminishing returns, with the potential for up to 8 dB sensitivity improvement at the 10^{-9} BER. In practice, much of this theoretical benefit can be realized, with demonstrated performance for the transceivers of Figure 7 and Figure 8 within ~1.5 dB of theory for 4-FSK and 8-FSK[35, 36]. From a sensitivity standpoint, the 4-FSK performance is comparable to the DPSK modulation that is planned for NASA's Laser Communications Relay Demonstration (LCRD) program[11, 17, 18]. But with 2-bits/symbol, 4-FSK requires only half the electrical bandwidth. The 8-FSK performance is another ~1.5 dB more sensitive, with demonstrated 10^{-9} BER sensitivity of 19 photons/bit. This is better than DPSK theory, and requires only ⅓ the electrical bandwidth, with the ability to deliver 7.5 Gbit/s with only 2.5 GHz electronic TX and RX bandwidth, and improved compatibility with photon-counting RXs. This experimental 8-FSK data point (circled in Figure 10) is noteworthy in that it is among the most sensitive real-time high-rate demonstrations reported without using FEC.

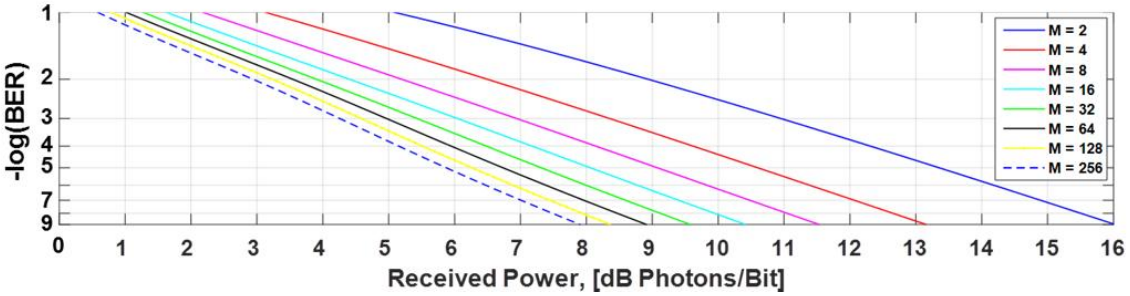

Figure 9. BER for ideal preamplifed *M*-ary orthogonal modulation.

Also significant is that when combined with moderate strength FEC, (e.g., 20% FEC with an error-free threshold of 1.7×10^{-2} BER), the theoretical performance of large *M*-orthogonal formats approaches that of the best reported photon-counting and coherent demonstrations using more powerful 100% overhead (rate-½) FEC.

Highlighted in Figure 10 is the theoretical performance of a 256-Orthogonal hybrid format with 2.5 GHz modulation bandwidth operating both with and without 20% overhead FEC. While large *M*-orthogonal modulation requires significant optical bandwidth expansion (relative to the data rate), low-power WDM channelization provides straightforward access to the optical spectrum. Given this and the challenge of implementing rate-½ FEC in real time at higher data rates > ~ 1 Gbit/s, it may be easier in practice to realize high-sensitivity performance at high data rates using *M*-orthogonal modulation and lower-overhead FEC than with alternative rate-½ approaches. Furthermore, by using hybrid *M*-orthogonal with a constant M_{eff} and fixed electrical bandwidth, the data rate may be varied up to a factor of M_{eff} by adjusting the ratio of *f* to *p,* without impacting receiver efficiency. For example, hybrid 256-orthogonal *f*-FSK/*p*-PPM with 2.5 GHz modulation bandwidth and 20% FEC can operate from 62.5 Mbit/s to 16 Gbit/s with a respectable theoretical sensitivity of ~2 photons/bit.

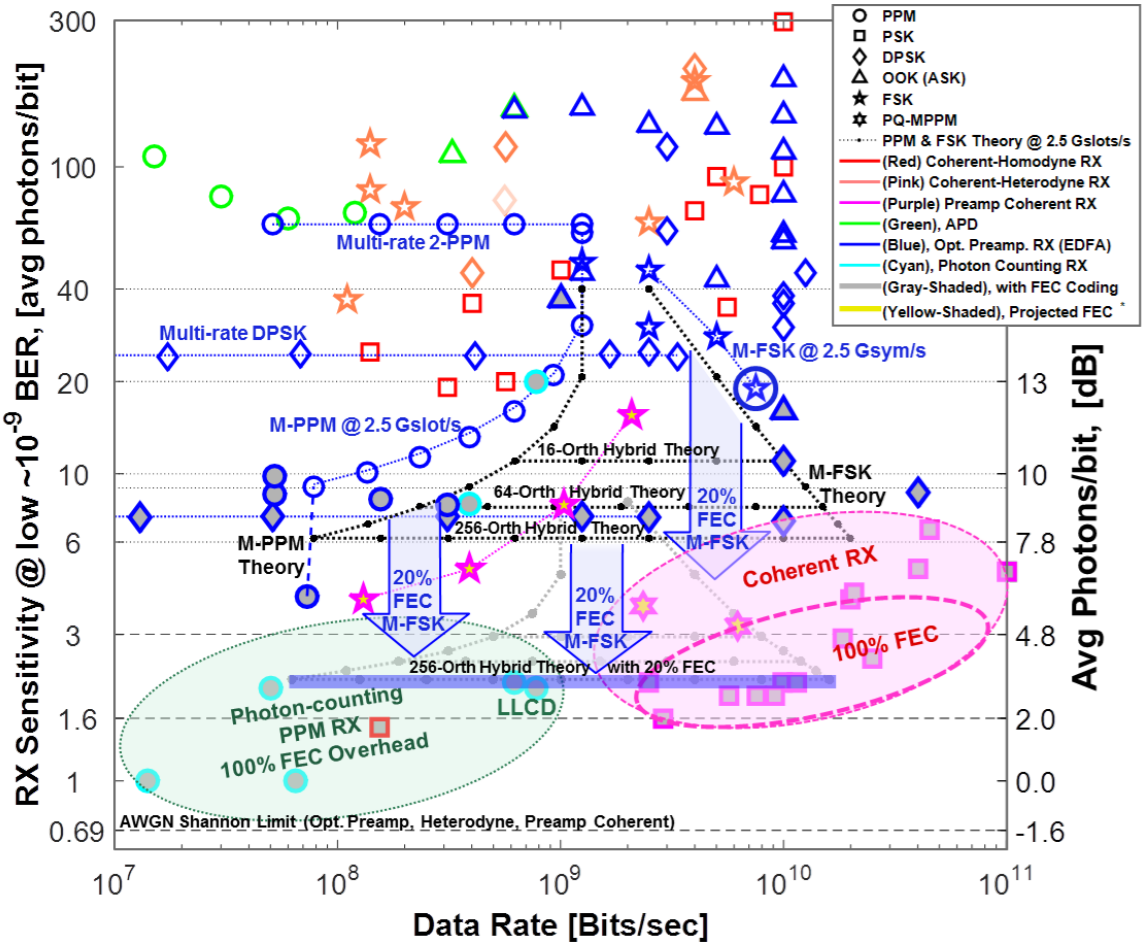

Figure 10. A sampling of high-sensitivity optical communication demonstrations showing reported sensitivities at low 10^{-9} BER as a function of data rate[5, 33, 45]. Modulation type is indicated by marker type, for instance PPM is represented by circles, FSK by stars. Receiver type is indicated by color: Red indicates coherent (dark red = homodyne and pink = heterodyne), dark blue indicates optically preamplified, and light-blue indicates a photon-counting RX. Coded demonstration results are shaded gray. On the lower-left-hand side, lower-speed photon-counting *M*-PPM RX performance with 100% FEC overhead is highlighted with 1-3 PPB sensitivity. On the lower-right-hand side, higher-speed preamplified coherent performance with ~2-6 PPB coded sensitivity is highlighted, along with the more sensitive coherent demonstrations with 100% FEC overhead in the ~2 – 4 PPB sensitivity range. Also shown are measured and theoretical performance curves for 2.5 GHz bandwidth *M*-PPM, *M*-FSK; theory curves for 2.5 GHz hybrid *p*-PPM/*f*-FSK for M_{eff} = 16, 64, and 256; and performance projections when used with 20% overhead FEC.

6. SUMMARY

Power-efficiency and flexibility are important design drivers for mobile free-space laser communication systems. The WDM-based transceivers we've described can provide efficient access to many THz of optical spectrum, with the potential for low-SWaP implementation and the ability to generate and receive a variety of high-sensitivity M-ary orthogonal modulations including PPM, FSK, and hybrid combinations. This provides a unique ability to adapt the transceiver parameters to accommodate electrical bandwidth or peak power limitations, and operate with high-photon-efficiency over a wide range of data rates, from the Mbit/s regime to many tens of Gbit/s. With these multi-rate multi-format capabilities, its possible that a single transceiver platform could operate efficiently over a sizeable portion of the rate-distance trade space of interest for future free-space applications, with systems ranging from small airborne or CubeSAT-sized communication payloads to larger interplanetary and deep-space lasercom platforms.

REFERENCES

[1] V. W. S. Chan, "Optical space communications," *IEEE Sel. Top. in Quantum Electronics,* vol. 6, pp. 959 - 975, (2000).

[2] J. R. Lesh, "Power Efficient Communications for Space Applications," in *International Telemetering Conference*, (1982).

[3] H. Hemmati, Ed. *Deep Space Optical Communiations*, (2006).

[4] A. Majumdar and J. C. Ricklin, Eds., *Free-Space Laser Communications: Principles and Advances* (2007).

[5] H. Hemmati and D. O. Caplan, "Optical Satellite Communications," in *Optical Fiber Telecommunications VI B*, I. Kaminow, T. Li, and A. E. Willner, Eds.: Elsevier, (2013).

[6] J. Taylor, D. K. Lee, and S. Shambayati, "Mars Reconnaissance Orbiter (MRO) Telecommunications," *DESCANSO Design and Performance Summary Series, Article 12,* (2006).

[7] S. A. Townes, F. Amoozegar, J. S. Border, J. C. Breidenthal, D. Morabito, K. I. Moyd, J. E. Patterson, and S. Shambayati, "Operational demonstration of Ka-band Telecommunications for the Mars Reconnaissance Orbiter," in *IEEE Aerospace Conference*, (2003).

[8] S. Shambayati, F. Davarian, and D. Morabito, "Link Design and Planning for Mars Reconnaissance Orbiter (MRO) Ka-band (32 GHz) Telecom Demonstration," in *IEEE Aerospace Conference*, (2005).

[9] S. A. Townes, et. al., "The Mars laser communication demonstration," *IEEE Aerospace Conf.* (2004).

[10] A. Biswas, D. Boroson, and B. Edwards, "Mars Laser Communication Demonstration: What it would have been," *Proc. SPIE, (Free-Space Laser Communication Technologies XVIII),* (2006).

[11] B. L. Edwards, D. Israel, K. Wilson, J. Moores, and A. Fletcher, "Overview of the Laser Communications Relay Demonstration Project," (2012).

[12] D. M. Boroson and B. S. Robinson "The Lunar Laser Communication Demonstration: NASA's First Step Toward Very High Data Rate Support of Science and Exploration Missions," *Space Science Reviews Journal,* (2014).

[13] M. Gregory, F. Heine, H. Kampfner, R. Meyer, R. Fields, and C. Lunde, "Tesat Laser Communication Terminal Performance Results On 5.6 Gbit Coherent Inter Satellite And Satellite To Ground Links," in *ICSO* Rhodes, Greece, (2010).

[14] H. Takenaka, Y. Koyama, M. Akioka, D. Kolev, N. Iwakiri, and Y. Munemasa, "In-orbit verification of small optical transponder (SOTA) evaluation of satellite-to-ground laser communication," *Proc. SPIE,* vol. 9739, (2016).

[15] N. W. Spellmeyer, D. O. Caplan, and M. L. Stevens, "Design of a 5-Watt PPM transmitter for the Mars Laser Communications Demonstration," in *LEOS*, (2005).

[16] S. Constantine, L. E. Elgin, M. L. Stevens, J. A. Greco, K. Aquino, D. D. Alves, and B. S. Robinson "Design of a High-Speed Space Modem for the Lunar Laser Communications Demonstration," *Proc. SPIE,* vol. 7923, (2011).

[17] D. O. Caplan, J. Carney, J. Fitzgerald, I. Gaschits, R. Kaminsky, G. Lund, S. Hamilton, R. Magliocco, R. Murphy, H. Rao, N. Spellmeyer, and J. Wang, "Multi-rate DPSK optical Transceivers for Free-space Applications," in *Proc. SPIE 8971*, (2014).

[18] N. W. Spellmeyer, C. Browne, D. Caplan, J. Carney, M. Chavez, A. Fletcher, J. Fitzgerald, R. Kaminsky, G. Lund, S. Hamilton, R. Magliocco, O. Mikulina, R. Murphy, H. Rao, M. Scheinbart, M. Seaver, and J. Wang, "A Multi-Rate Modem for Free-Space Laser Communications," in *Proc. SPIE 8971*, (2014).
[19] R. W. Kingsbury, D. O. Caplan, and K. L. Cahoy, "Compact Optical Transmitters for CubeSat Free-Space Optical Communications," *Proc. SPIE 9354-27,* (2015).
[20] R. W. Kingsbury, D. O. Caplan, and K. L. Cahoy, "Implementation and validation of a CubeSat laser transmitter," *Proc. SPIE,* vol. 9739, (2016).
[21] T. S. Rose, R. P. Welle, D. W. Rowen, and S. W. Janson, "Laser downlink demonstration from a 1.5U CubeSat," *Proc. SPIE,* vol. 9739, (2016).
[22] R. Essiambre, G. Kramer, P. J. Winzer, G. J. Foschini, and B. Goebel, "Capacity Limits of Optical Fiber Networks," *J. Lightwave Tech.,* vol. 28, pp. 662-701, (2010).
[23] J. M. Ross, S. I. Green, and J. Brand, "Short-pulse optical communication experiments," *Proc. IEEE,* vol. 58, (1970).
[24] J. R. Pierce, "Optical Channels: Practical Limits with Photon Counting," *IEEE Trans. Commun. ,* vol. COM-26, pp. 1819-1821, (1978).
[25] J. R. Pierce, E. C. Posner, and E. R. Rodemich, "The Capacity of the Photon Counting Channel," *IEEE Trans. Information Theory,* vol. IT-27, pp. 61-77, (1981).
[26] J. R. Lesh, "Capacity Limit of the Noiseless, Energy-Efficient Optical PPM Channel," *IEEE Trans. Comm.,* vol. 31, pp. 546 - 548, (1983).
[27] D. O. Caplan, B. S. Robinson, R. J. Murphy, and M. L. Stevens, "Demonstration of 2.5-Gslot/s optically-preamplified M-PPM with 4 photons/bit receiver sensitivity," in *Optical Fiber Conference (OFC), Paper PDP23* (2005).
[28] B. S. Robinson, D. O. Caplan, M. L. Stevens, R. J. Barron, E. A. Dauler, and S. A. Hamilton, "1.5-photons/bit Photon-Counting Optical Communications Using Geiger-Mode Avalanche Photodiodes," in *IEEE LEOS Summer Topical Meetings*, (2005).
[29] B. S. Robinson, A. J. Kerman, E. A. Dauler, R. J. Barron, D. O. Caplan, M. L. Stevens, J. J. Carney, S. A. Hamilton, J. K. W. Yang, and K. K. Berggren, "781-Mbit/s Photon-Counting Optical Communications Using Superconducting NbN-Nanowire Detectors," *Opt. Lett.,* vol. 31, pp. 444-446, (2006).
[30] J. A. Mendenhall, L. M. Candell, P. I. Hopman, G. Zogbi, D. M. Boroson, D. O. Caplan, C. J. Digenis, D. R. Hearn, and R. C. Shoup, "Design of an Optical Photon Counting Array Receiver System for Deep Space Communications," *Proc. IEEE,* vol. 95, pp. 2059-2069, (2007).
[31] D. O. Caplan, "A technique for measuring and optimizing modulator extinction ratio," in *CLEO*, (2000).
[32] M. Pauer and P. J. Winzer, "Impact of Extinction Ratio on Return-to-Zero Coding Gain in Optical Noise Limited Receivers," *IEEE Photon. Technol. Lett.,* vol. 15, pp. 879 - 881, (2003).
[33] D. O. Caplan, "Laser Communication Transmitter and Receiver Design," in *Free-Space Laser Communications: Principles and Advances*, A. Majumdar and J. C. Ricklin, Eds.: Springer, (2007).
[34] D. O. Caplan, J. J. Carney, R. E. Lafon, and M. L. Stevens, "Design of a 40 Watt 1.55μm uplink transmitter for Lunar Laser Communications," *Proc. SPIE* 8246 (2012).
[35] D. O. Caplan, J. J. Carney, and S. Constantine, "Parallel Direct Modulation Laser Transmitters for High-speed High-sensitivity Laser Communications," *Conference on Lasers and Electro-Optics (CLEO), Postdeadline Paper PDPB12* (2011).
[36] D. O. Caplan and J. Carney, "Power-efficient Noise-insensitive Optical Modulation for High-sensitivity Laser Communications," *CLEO,* (2014).
[37] D. O. Caplan, "Method and Apparatus for Transmitting Optical Signals," Patent no. 8,073,342, (2011).
[38] D. O. Caplan, B. S. Robinson, M. L. Stevens, D. M. Boroson, and S. A. Hamilton, "High-Rate Photon-Efficient Laser Communications with Near Single Photon/bit Receiver Sensitivities," in *OFC*, (2006).
[39] D. M. Boroson, "A survey of technology-driven capacity limits for free-space laser communications " *SPIE Proc.* (2007).
[40] D. O. Caplan, M. L. Stevens, D. M. Boroson, and J. E. Kaufmann, "A multi-rate optical communications architecture with high sensitivity," in *LEOS*, (1999).
[41] R. T. Schulein, R. E. Lafon, M. B. Taylor, P. A. MacKoul, J. J. Carney, M. L. Stevens, B. S. Robinson , S. Constantine, M. M. Willis, D. W. Peckham, B. Zhu, J. M. Fini, and D. O. Caplan, "Nonlinearity mitigation of a 40-Watt 1.55-micron uplink transmitter for lunar laser communications," *Proc. SPIE, Free-Space Laser Communication and Atmospheric Propagation XXV* 8610 (2013).

[42] M. M. Willis, A. J. Kerman, M. E. Grein, J. Kansky, B. R. Romkey, E. A. Dauler, D. Rosenberg, B. S. Robinson, D. V. Murphy, and D. M. Boroson, "Performance of a Multimode Photon-Counting Optical Receiver for the NASA Lunar Laser Communications Demonstration," in *International Conference on Space Optical Systems and Applications (ICSOS)* Corsica, France, (2012).
[43] P. Wysocki, T. Wood, A. Grant, D. Holcomb, K. Chang, M. Santo, L. Braun, and G. Johnson, "High Reliability 49 dB Gain, 13W PM Fiber Amplifier at 1550 nm with 30 dB PER and Record Efficiency," in *OFC, paper PDP17*, (2006).
[44] E. Y. Luzhansky, D. Israel, and B. Edwards, "Laser communication relay demonstration," *Proc. SPIE,* vol. 9739, (2016).
[45] S. B. Alexander, *Optical communication receiver design*. Bellingham, Washington, USA: SPIE Opt. Eng. Press, (1997).
[46] M. Shirasaki, H. Nishimoto, T. Okiyama, and T. Touge, "Fibre transmission properties of optical pulses produced through direct phase modulation of DFB laser diode," *Electron. Lett.,* vol. 24, pp. 486-488, (1988).
[47] R. S. Vodhanel, A. F. Elrefaie, M. Z. Iqbal, R. E. Wagner, J. L. Gimlett, and S. Tsuji, "Performance of directly modulated DFB lasers in 10-Gb/s ASK, FSK, and DPSK lightwave systems," *J. Lightwave Tech.,* vol. 8, pp. 1379 - 1386, (1990).
[48] D. Mahgerefteh, P. S. Cho, J. Goldhar, and H. I. Mandelberg, "Penalty-free propagation over 600 km of nondispersion shifted fiber at 2.5 Gb/s using a directly laser modulated transmitter," in *CLEO*, (1999).
[49] S. Chandrasekhar, C. R. Doerr, L. L. Buhl, Y. Matsui, D. Mahgerefteh, X. Zheng, K. McCallion, Z. Fan, and P. Tayebati, "Repeaterless Transmission With Negative Penalty Over 285 km at 10 Gb/s Using a Chirp Managed Laser," *Photonics Tech. Lett.,* vol. 17, pp. 2454-2457, (2005).
[50] S. J. Spector, J. M. Knecht, R. T. Schulein, and D. O. Caplan, "Silicon Photonic Filters for Compact High Extinction Ratio Power Efficient (CHERPe) Transmitters," *Conference on Lasers and Electro-optics (CLEO),* (2015).
[51] Pat. pending.